Chinese Journal of Physics 56 (2018) 1252–1261

Contents lists available at ScienceDirect

Chinese Journal of Physics

journal homepage: www.elsevier.com/locate/cjph

Spin-1/2 Ising model on a AFM/FM two-layer Bethe lattice in a staggered magnetic field

J. Kplé[a,b], S. Massou[a], F. Hontinfinde[*,a,b], E. Albayrak[c]

[a] Department of Physics, University of Abomey-Calavi, Benin
[b] Institute of Mathematic and Physical Sciences (IMSP), Benin
[c] Department of Physics, Erciyes University, Kayseri 38039, Turkey

ARTICLE INFO

Keywords:
Phase transitions
Spin-1/2 Ising model
Bilayer Bethe lattice
Ground states phase diagrams
Exact recursion relations
Second-order phase boundaries

ABSTRACT

A bilayer spin-1/2 Ising model consisting of two superposed Bethe lattices with antiferromagnetic/ferromagnetic interactions is studied by the use of exact recursion relations in a pairwise approach in the presence of an external staggered magnetic field. Besides the ground state phase diagrams calculated in different possible planes of the model parameters space, the thermal variations of the order-parameters and the free energy are investigated to obtain the temperature-dependent phase diagrams of the model for different values of the coordination numbers q. Our calculations reveal that depending on the strength of the model parameters, the model exhibits a variety of interesting phase transitions and therefore phase diagrams.

1. Introduction

The study of the magnetic properties of ultra-thin film, multilayer and superlattice systems attracted much interest from physicists in recent years due to their possible technological applications [1–4]. Indeed, materials consisting of multiple layers of different magnetic substances have been recently thoroughly investigated for both theoretical and experimental motivations. These systems offer challenging opportunities to elaborate materials with novel magnetic properties, such as giant magnetoresistance [5], surface magnetic anisotropy [6], and surface magnetoelastic coupling [7], etc. Experimentally, several works have been performed related to magnetic multilayers such as FeF_2 [8], $Fe/KCoF_3$ [9], $Co/Cu/Ni_{80}Fe_{20}$ [10], Co/Cu/FeMn [11] and FePt/Fe [12]. From the theoretical point of view, thin films have been treated within several different frameworks: mean field theory (MFT), a generalized MFT, a scaling approach and high-temperature series expansion [13], effective-field theory [14], two-site cluster approximation [15], Monte Carlo techniques [16], spin-fluctuation theory [17], renormalization group techniques [18] and in terms of exact recursion relations (ERR's) in a pairwise approach on the Bethe lattice (BL) [19–24]. Thus, much effort has been devoted to investigate the criticality and other statistical properties in view to get a deeper understanding of order-disorder phase transitions [25].

The present work deals with the magnetic properties of a spin-1/2 Ising model on a two-layer BL under an external staggered magnetic field (ESMF). The ERR's in a pairwise approach are employed in our calculations [19–24]. This technique has been early considered by Albayrak et al. in the case of an uniform magnetic field [20]. Here, instead of using the uniform one, an alternating external magnetic field, i.e. $+H$ and $-H$, acting on the even and odd sublattices respectively are assumed. Therefore, new types of phase diagrams due to new phases are generated.

The outline of this paper is as follows. In Section 2, the model and formalism are presented. In Section 3, results and discussions are given. Finally, Section 4 contains the conclusion.

* Corresponding author.
E-mail address: felix.hontinfinde@fast-uac.bj (F. Hontinfinde).

https://doi.org/10.1016/j.cjph.2018.04.008
Received 5 December 2017; Received in revised form 3 April 2018; Accepted 3 April 2018
Available online 12 April 2018

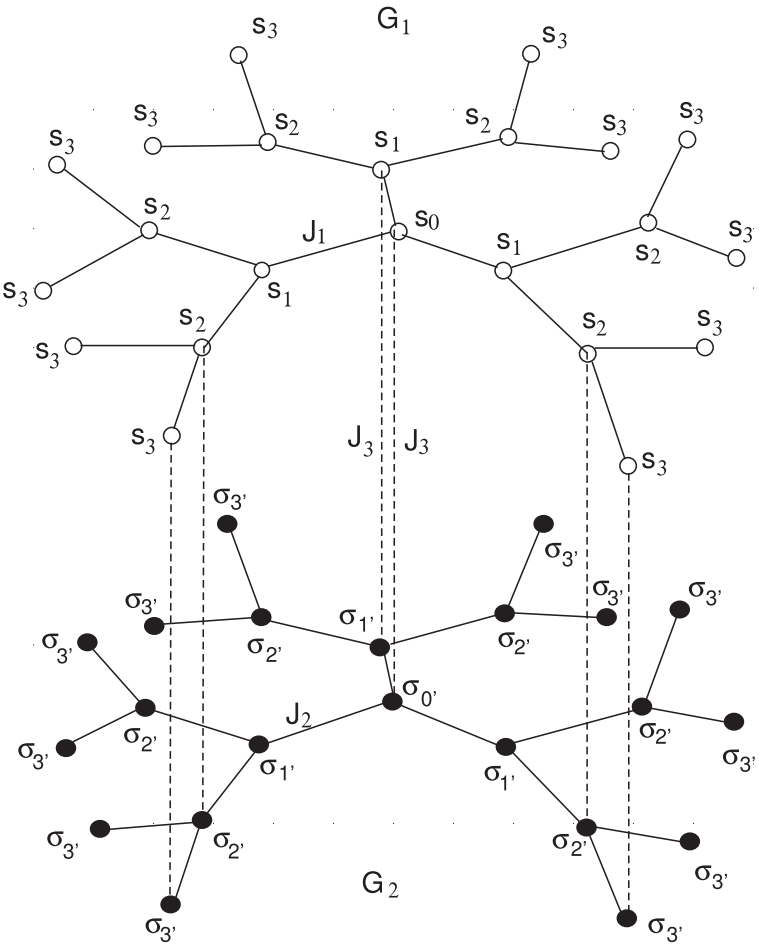

Fig. 1. The two-layer BL. G_1 and G_2 refer to the upper and lower layers having the spins labeled as S_i, S_j and $\sigma_{i'}$, $\sigma_{j'}$. J_1 and J_2 correspond respectively to the bilinear interactions of spins in G_1 and G_2, while J_3 is the one for the adjacent spins of G_1 and G_2.

2. The model and its formulation

The critical properties of spin-1/2 Ising model on a two-layer BL G_1 and G_2 with antiferromagnetic/ferromagnetic (AFM/FM) intralayer and either FM or AFM type of interlayer interactions are studied in the presence of an ESMF. The pairwise approach is employed for this investigation [19–24].

In this approach, an adjacent nearest-neighbor (NN) pair is picked from deep inside the two-layer lattice; this constitutes the central pair, which forms the first-generation spins. This pair of spins is connected to q NN spin pairs (q is the coordination number), which form the second-generation spins. Each pair of spins in the second generation is joined to $(q-1)$ NN's. Hence, in total, the second generation has $q(q-1)$ NN spins that form the third generation of spins and so on to infinity (see Fig 1). Thus, each spin has $(q+1)$ NN spins, q from its own layer and one from the adjacent layer.

The Ising Hamiltonian of such a two-layer BL may be given as

$$\mathscr{H} = -J_1 \sum_{<ij>} S_i S_j - J_2 \sum_{<i'j'>} \sigma_{i'}\sigma_{j'} - J_3 \sum_{<ii'>} S_i \sigma_{i'} - \sum_{i} H_i S_i - \sum_{i'} H_{i'}\sigma_{i'} \tag{1}$$

where $S_i = \pm 1/2$ and $\sigma_{i'} = \pm 1/2$ indicate the spin variables at sites i and i' on G_1 and G_2. J_1 and J_2 are the intralayer NN exchange interactions of the layers and the first and second summations are carried out only over all adjacent NN pairs of spins in G_1 and G_2, respectively. J_3 is the interlayer bilinear interaction of adjacent NN spins between the layers, therefore, the third summation runs over all adjacent neighboring sites of G_1 and G_2. H_i and $H_{i'}$ denote magnetic fields acting on the sites i and i' respectively. The staggered field is obtained by setting $H_i = H_{i'} = H$ if i and i' are in the even sublattice and $H_i = H_{i'} = -H$ if i and i' are in the odd sublattice of both G_1 and G_2.

The partition function is the essential part of the formulation that yields a formulation in terms of ERR's. It is defined as

$$\mathbb{Z} = \sum_{\{c\}} e^{-\beta\mathscr{H}} = \sum_{Spc} P(Spc) \tag{2}$$

where $\{c\}$ denotes all system configurations, $P(Spc)$ is the unnormalized probability distribution [26], $\beta = 1/kT$ is the inverse temperature with k being the Boltzmann constant. When one considers the central pair and the NN pairs, the $P(Spc)$'s can be found respectively as

$$P(\{S_0, \sigma_{0'}\}) = e^{\beta[J_3 S_0 \sigma_{0'} + H(S_0 + \sigma_{0'})]} \prod_{j=1}^{q} Q_n[\{S_0, \sigma_{0'}\}|(S, \sigma)^j], \tag{3}$$

and

$$P(\{S_1, \sigma_{1'}\}) = e^{\beta[J_3 S_1 \sigma_{1'} - H(S_1 + \sigma_{1'})]} \prod_{k=1}^{q} Q_{n-1}[\{S_1, \sigma_{1'}\}|(S, \sigma)^k], \tag{4}$$

where $(S, \sigma)^j$ corresponds to the pair of spins of the jth sub-tree other than the central pair (S_0, σ_0) [24,27] and so on. The suffix n refers to the fact that the sub-tree has n-shells, i.e. n steps from root to boundary sites where

$$\begin{aligned} Q_n[\{S_0, \sigma_{0'}\}|(S, \sigma)^j] &= e^{\beta[J_1 S_0 S_1 + J_2 \sigma_{0'} \sigma_{1'} + J_3 S_1 \sigma_{1'} - H(S_1 + \sigma_{1'})]} \\ &\times e^{\beta\left[J_1 \sum_{\langle i,j\rangle} S_i S_j + J_2 \sum_{\langle i'j'\rangle} \sigma_{i'} \sigma_{j'} + J_3 \sum_{\langle ii'\rangle} S_i \sigma_{i'} + \sum_{\langle ii'\rangle} (H_i S_i + H_{i'} \sigma_{i'})\right]}. \end{aligned} \tag{5}$$

Thus,

$$Q_n[\{S_0, \sigma_{0'}\}|(S, \sigma)^j] = e^{\beta[J_1 S_0 S_1 + J_2 \sigma_{0'} \sigma_{1'} + J_3 S_1 \sigma_{1'} - H(S_1 + \sigma_{1'})]} \prod_{k=1}^{q-1} Q_{n-1}[(S_1, \sigma_{1'})^j|(S, \sigma)^k] \tag{6}$$

where $(S, \sigma)^k$ denotes all pairs of spin configurations (other than $(S_1, \sigma_{1'})^j$) on the kth branch of the sub-tree.

Advancing along any branch, one gets

$$Q_{n-1}[(S_1, \sigma_{1'})^j|(S, \sigma)^k] = e^{\beta[J_1 S_1 S_2 + J_2 \sigma_{1'} \sigma_{2'} + J_3 S_2 \sigma_{2'} + H(S_2 + \sigma_{2'})]} \prod_{l=1}^{q-1} Q_{n-2}[(S_2, \sigma_{2'})^k|(S, \sigma)^l] \tag{7}$$

where $(S, \sigma)^l$ indicates all spins pairs (other than $(S_2, \sigma_{2'})^k$) on the next lth branch of the upper subsub-tree.

Let us define

$$g_n(S_0, \sigma_{0'}) = \sum_{\{S_1, \sigma_{1'}\}} Q_n(\{S_0, \sigma_{0'}\}|(S, \sigma)). \tag{8}$$

Using Eq. (6) and summing over all $\{S_1, \sigma_{1'}\}$, one gets

$$g_n(S_0, \sigma_{0'}) = \sum_{\{S_1, \sigma_{1'}\}} e^{\beta[J_1 S_0 S_1 + J_2 \sigma_{0'} \sigma_{1'} + J_3 S_1 \sigma_{1'} - H(S_1 + \sigma_{1'})]} [g_{n-1}(S_1, \sigma_{1'})]^{q-1}. \tag{9}$$

Similarly, by using Eq. (7) we also obtain

$$g_{n-1}(S_1, \sigma_{1'}) = \sum_{\{S_2, \sigma_{2'}\}} e^{\beta[J_1 S_1 S_2 + J_2 \sigma_{1'} \sigma_{2'} + J_3 S_2 \sigma_{2'} + H(S_2 + \sigma_{2'})]} [g_{n-2}(S_2, \sigma_{2'})]^{q-1}. \tag{10}$$

Since S_i and $\sigma_{i'}$ can take the values $\pm 1/2$, one can define four $g_n(S, \sigma)$ functions. The ERR's in terms of the ratios of the g_n functions read as

$$X_n = \frac{g_n\left(+\frac{1}{2}, +\frac{1}{2}\right)}{g_n\left(-\frac{1}{2}, -\frac{1}{2}\right)}, \qquad Y_n = \frac{g_n\left(+\frac{1}{2}, -\frac{1}{2}\right)}{g_n\left(-\frac{1}{2}, -\frac{1}{2}\right)}, \qquad Z_n = \frac{g_n\left(-\frac{1}{2}, +\frac{1}{2}\right)}{g_n\left(-\frac{1}{2}, -\frac{1}{2}\right)}. \tag{11}$$

The magnetizations M_1 and M_2 of layers G_1 and G_2, respectively, are the order parameters defined as:

$$M_1 = \langle S \rangle = \frac{1}{N} \sum_{i=1}^{N} \langle S_i \rangle \qquad \text{and} \qquad M_2 = \langle \sigma \rangle = \frac{1}{N} \sum_{i'=1}^{N} \langle \sigma_{i'} \rangle \tag{12}$$

where $\langle ... \rangle$ denotes the usual thermal average. $\langle S_0 \rangle$ and $\langle \sigma_{0'} \rangle$ can be expressed in terms of the ERR's as:

$$\langle S_0 \rangle = \left[e^{\beta(0.25 J_3 + H)} X_n^q + e^{-\beta(0.25 J_3)} Y_n^q - e^{-\beta(0.25 J_3)} Z_n^q - e^{\beta(0.25 J_3 - H)}\right] / 2\mathbb{Z} \tag{13}$$

and

$$\langle \sigma_{0'} \rangle = \left[e^{\beta(0.25 J_3 + H)} X_n^q - e^{-\beta(0.25 J_3)} Y_n^q + e^{-\beta(0.25 J_3)} Z_n^q - e^{\beta(0.25 J_3 - H)}\right] / 2\mathbb{Z} \tag{14}$$

with

$$\mathbb{Z} = e^{\beta(0.25 J_3 + H)} X_n^q + e^{-\beta(0.25 J_3)} Y_n^q + e^{-\beta(0.25 J_3)} Z_n^q + e^{\beta(0.25 J_3 - H)} \tag{15}$$

It is important to notice that depending on the strength of different magnetic interactions, the system could globally be antiferromagnetic or ferromagnetic. In each of these two cases, the total magnetization is written in the form,

$$M = \frac{1}{2}(M_1 + M_2) \tag{16}$$

since the signs of M_1 and M_2 are already handled by alternately changing sign of the external magnetic field H. In order to calcultate M_1 and M_2, one needs to know the magnetic structure of the whole lattice which depends on selected values of model parameters.

The free energy of the system is obtained using Eqs. (2) and (9)–(11) and the definition $F = -kT \ln \mathbb{Z}$. It is calculated to be

$$\begin{aligned} -\beta F &= \frac{q-1}{2-q}\ln[e^{\beta(-0.25J_1-0.25J_2+0.25J_3+H)}X_n^{q-1} + e^{\beta(-0.25J_1+0.25J_2-0.25J_3)}Y_n^{q-1} \\ &+ e^{\beta(0.25J_1-0.25J_2-0.25J_3)}Z_n^{q-1} + e^{\beta(0.25J_1+0.25J_2+0.25J_3-H)}] \\ &+ \ln\left[e^{\beta(0.25J_3+H)}X_n^{q} + e^{\beta(-0.25J_3)}Y_n^{q} + e^{\beta(-0.25J_3)}Z_n^{q} + e^{\beta(0.25J_3-H)}\right] \\ &+ \frac{1}{2-q}\ln[e^{\beta(-0.25J_1-0.25J_2+0.25J_3-H)}X_{n-1}^{q-1} + e^{\beta(-0.25J_1+0.25J_2-0.25J_3)}Y_{n-1}^{q-1} \\ &+ e^{\beta(0.25J_1-0.25J_2-0.25J_3)}Z_{n-1}^{q-1} + e^{\beta(0.25J_1+0.25J_2+0.25J_3+H)}] \end{aligned} \tag{17}$$

Since each layer is divided into two sublattices A and B, such that every site belonging to A is only surrounded by sites belonging to B and vice versa, to account the two-sublattice structure, the ERR's may therefore be written as [20]:

$$\{X_n, Y_n, Z_n\} \longrightarrow \begin{cases} \{X_n^{\mathrm{A}}, Y_n^{\mathrm{A}}, Z_n^{\mathrm{A}}\} & \text{for even } n, \\ \{X_n^{\mathrm{B}}, Y_n^{\mathrm{B}}, Z_n^{\mathrm{B}}\} & \text{for odd } n. \end{cases}$$

Indeed, important points of this approach are that non-staggered phases are described by the single fixed points $\{X_n, Y_n, Z_n\} \to \{X, Y, Z\}$, while staggered phases appear as two-cycle double points [28] as indicated above. Thus, the sublattice magnetizations for layers G_1 and G_2, because each spin only interacts with its NN's from its own layer and a NN from the adjacent layer with the same sublattice, i.e., A or B, can be written as [20,24]:

$$\{M_{1,2}\} \longrightarrow \begin{cases} \{M_{1\mathrm{A}}, M_{2\mathrm{A}}\} & \text{for even } n, \\ \{M_{1\mathrm{B}}, M_{2\mathrm{B}}\} & \text{for odd } n. \end{cases}$$

where, 1 and 2 refer to layers G_1 and G_2, while A and B refer to sublattices.

The free energy is obtained as:

$$\{F_n\} \longrightarrow \begin{cases} \{F_n^{\mathrm{A}}\} & \text{for even } n, \\ \{F_n^{\mathrm{B}}\} & \text{for odd } n. \end{cases}$$

3. The ground states phase diagrams

The determination of stable phases at $T = 0$ requires the calculation of the ground state (GS) energy of the system. The GS configurations are those having the lowest energy depending on values of interaction parameters.

The GS energies are obtained from Eq. (1) in units of $|J_k|$ by rewriting it in the following form:

$$\frac{E}{q|J_k|} = -\sum_{\langle plaq\rangle}\left[\frac{J_1}{|J_k|}S_iS_j + \frac{J_2}{|J_k|}\sigma_{i'}\sigma_{j'} + \frac{J_3}{q|J_k|}(S_i\sigma_{i'} + S_j\sigma_{j'}) + \frac{H}{q|J_k|}(S_i + \sigma_{i'} - S_{j'} - \sigma_{j'})\right], \tag{18}$$

where $k = 1$ or 2 and the summation goes over all plaquettes which consist of four NN pairs of the system, with one pair $\langle ij\rangle$ from G_1, one pair $\langle i'j'\rangle$ from G_2, and two pairs $\langle ii'\rangle$ and $\langle jj'\rangle$ connecting G_1 and G_2. By comparing the values of the energy for different spin configurations, the GS phase diagrams are obtained.

By symmetry considerations, only the positive values of $H/q|J_k|$ are taken into account. For negative values of $H/q|J_k|$, the relation $|M(-H)| = |-M(H)| = |M(H)|$ holds. Five different types of GS configurations for a central plaquette deep inside the two-layer BL are obtained: The FM phase (I); a compensated phase (II) with layers of FM type but interactions between them is AFM type; the surface FM phase (III), i.e. layers G_1 and G_2 are AFM and FM type respectively; a mixed phase (IV), with AFM intralayer and FM interlayer interactions on the layers and the AFM phase (V) i.e. the case where the interactions in both layers and between them are of antiferromagnetic type (see Table 1).

It should be noted that some of these GS configurations have been obtained in Ref. [20] in cases of AFM/AFM and FM/AFM interactions in an uniform magnetic field environment. From the previous GS configurations, one easily constructs the GS phase diagrams. The relevant GS diagrams including all available GS's are displayed in Fig. 2.

In Fig. 2a, the GS phase diagram on the $(J_2/|J_1|, J_3/q|J_1|)$ plane is calculated for $H/q|J_1| = 0.5$ and that of the inset for $H/q|J_1| = 1.0$. It is easy to see that all GS phases configurations are present. The boundary line separating phases (I) and (IV) appears to be more sensitive to changes in $H/q|J_1|$ than in $J_2/|J_1|$. Thus, increasing the values of $H/q|J_1|$ enlarges the stability of the mixed

Table 1
The GS configurations. Phases are indicated with (S_0, S_1) and ($\sigma_{0'}$, $\sigma_{1'}$) NN pairs for layers G_1 and G_2 respectively, with the GS spin values of 1/2.

I	± 1/2 ± 1/2 ± 1/2 ± 1/2	II	± 1/2 ± 1/2 ∓1/2 ∓1/2
III	+ 1/2 − 1/2 ± 1/2 ± 1/2	IV	+ 1/2 − 1/2 + 1/2 − 1/2
V	± 1/2 ∓1/2 ∓1/2 ± 1/2		

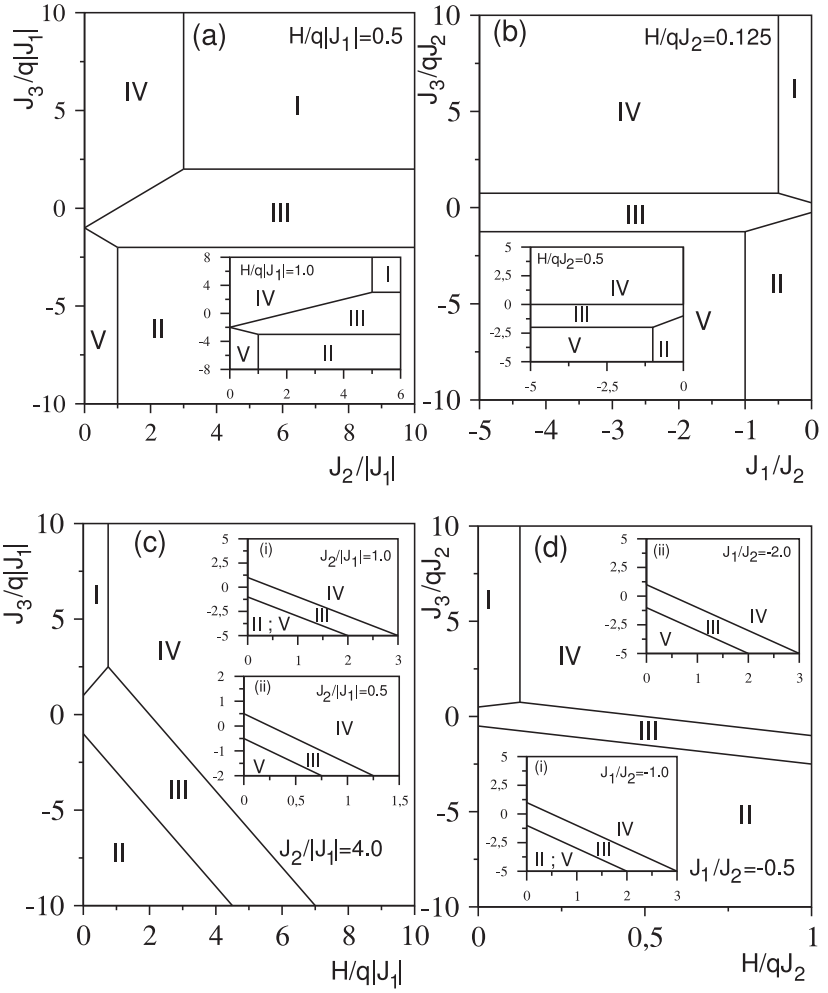

Fig. 2. The GS phase diagrams of the spin-1/2 Ising model on a AFM/FM two-layer BL on the ($J_2/|J_1|$, $J_3/q|J_1|$) plane for $H/q|J_1| = 0.5$ and in the inset for $H/q|J_1| = 1.0$ (a); on the (J_1/J_2, J_3/qJ_2) plane for $H/qJ_2 = 0.125$ and in the inset for $H/qJ_2 = 0.5$ (b); on the ($H/q|J_1|$, $J_3/q|J_1|$) plane for $J_2/|J_1| = 4.0$ and in the insets (*i*) and (*ii*) for respectively $J_2/|J_1| = 1.0$ and $J_2/|J_1| = 0.5$ (c); on the (H/qJ_2, J_3/qJ_2) plane for $J_1/J_2 = -0.5$ and in the insets (*i*) for $J_1/J_2 = -1.0$ and (*ii*) for $J_1/J_2 = -2.0$ (d).

phase (IV). The phase boundary between the compensated phase (II) and the antiferromagnetic phase (V) is always represented by straight vertical lines $J_2/|J_1| = 1.0$. This reflects its independence of the staggered magnetic field. One finds that phase (III) always appears as an intermediate phase between phases (I), (IV) and (II), (V) and develops for moderate values of $J_3/q|J_1|$. These GS phase diagrams could be divided into three regions for given values of $H/q|J_1|$. The first one is defined through the inequality: $J_2/|J_1| > 1 + 4H/q|J_1|$. There, phase (III) is confined between phases (I) and (II) in the region defined by: $-1 - 2H/q|J_1| \leqslant J_3/q|J_1| \leqslant 1 + 2H/q|J_1|$. The second one is defined through $1 < J_2/|J_1| < 1 + 4H/q|J_1|$. There, phase (I) disappears and a mixed phase (IV) appears. The GS configuration (III), is actually separated from phases (II) and (IV) by boundary lines $1 + J_3/q|J_1| + 2H/q|J_1| = 0$ and $J_2/|J_1| - J_3/q|J_1| - 2H/q|J_1| = 0$ respectively. The third one is define by $0 < J_2/|J_1| < 1$. In this region,

phase (III) still exist and is actually contained in a domain separating phases (IV) and (V) by boundary lines $J_2/|J_1|-J_3/q|J_1| - 2H/q|J_1| = 0$ and $J_2/|J_1|+J_3/q|J_1| + 2H/q|J_1| = 0$ respectively. This region which has a triangular form is symmetric along the axis $J_3/q|J_1| = -2H/q|J_1|$.

In Fig. 2b, one can see the GS phase diagram on the (J_1/J_2, J_3/qJ_2) plane for $H/qJ_2 = 0.125$. That of the inset is displayed for $H/qJ_2 = 0.5$. It is quite evident that all five GS configurations can be realized depending of values of the ESMF. The GS spin arrangement (I) does not exist for $H/qJ_2 \geq 0.25$. Under this condition, the GS spin arrangement (IV) spreads up. This results from a high interaction of spins with the external field. It should be also noted that phases compatible with small positive values of $J_2/|J_1|$ in the previous case (Fig. 2a), now correspond to large negative values of J_1/J_2 and vice-versa.

The next GS phase diagrams displayed in Fig. 2c, are obtained on the ($H/q|J_1|$, $J_3/q|J_1|$) plane for $J_1/J_2 = 4.0$ and in inset panels (*i*) and (*ii*) for $J_2/J_1 = 1.0$ and 0.5 respectively. One distinguishes the following situation: For $0 < J_2/J_1 < 1$, only three GS configurations, namely (III), (IV) and (V) appear. The phase (III) occupies a region between phases (IV) and (V), separated from them by respectively boundaries lines $J_2/|J_1|-J_3/q|J_1| - 2H/q|J_1| = 0$ and $J_2/|J_1|+J_3/q|J_1| + 2H/q|J_1| = 0$ respectively, as may be seen in the inset panel (*ii*) of Fig. 2c. For $J_2/J_1 = 1$, the inset (*i*) shows that phase (II) is also seen in addition to other three phases and it coexists with phase (V). Phase (III) is actually contained in a region separating phases (IV) and (II, V) by lines of equations, $1 - J_3/q|J_1| - 2H/q|J_1| = 0$ and $1 + J_3/q|J_1| + 2H/q|J_1| = 0$ respectively; For $J_2/J_1 > 1$, phases (II) and (V) do not coexist anymore and only phase (II) survives. Phase (I) is also seen in addition to phases (II), (III) and (IV), as can be seen in the main figure.

We show in Fig. 2d, the GS phase diagrams in the (H/qJ_2, J_3/qJ_2) plane for $J_1/J_2 = -0.5$ and in the inset panels (*i*) and (*ii*) for $J_1/J_2 = -1.0$ and -2.0 respectively. The topology of these phase diagrams is also analogous to those displayed in Fig. 2c.

These GS phase diagrams show similar trends with those of the spin-3/2 Ising model on a two-layer BL with FM/AFM interactions reported in Ref. [23].

4. Temperature phase diagrams

Before going into the discussion about the temperature-dependent phase diagrams, it is instructive to provide some insight into the thermal variations of the order parameters. Fig. 3a,b are obtained for $H/q|J_1| = 0.5$ and $J_3/q|J_1| = -4.0$ when the values of $J_2/|J_1|$ are set to 2.0 and 0.5, respectively. It is obvious from Fig. 3a that the system undergoes a second-order phase transition from the phase (II) to the paramagnetic phase (P). Indeed, at $T = 0$, $M_{1A} = M_{1B} = 0.5$ and $M_{2A} = M_{2B} = -0.5$ and as the temperature increases sublattice magnetizations remain inseparable and go to zero continuously. Fig. 3b illustrates the second-order phase transition from the AFM phase (V) to the paramagnetic phase (P). Indeed, at $T = 0$, $M_{1A} = M_{2B} = 0.5$ and $M_{1B} = M_{2A} = -0.5$. With the increase in temperature, sublattice magnetizations decrease and go to zero at the transition temperature T_N. Fig. 3c illustrates that for $H/q|J_1| = 0.5$ and $J_3/q|J_1| = -4.0$, sublattice magnetizations drop to zero in the region $0.559 < J_2/|J_1| < 1.441$.

Our numerical calculations indicate that displayed phase boundaries are of second-order and the ordered (disordered) phases are located below (above) depicted critical lines. At T_N, the total magnetization and the layer magnetizations vanish. The temperature-dependent phase diagrams are calculated for $q = 3$, 4 and 6 and associated phase transition lines are labeled with dotted, dashed and solid lines, respectively. Arrows in the figures indicate the phase separation points according to the GS phase diagrams.

Phase diagrams in the ($J_3/|J_1|$, $kT/|J_1|$) plane are shown in Fig. 4a–c for $H/q|J_1| = 0.5$ and for selected values of $J_2/|J_1|$: 4.0, 2.0 and 0.5:

(*i*)- In Fig. 4a, we have plotted the variation of the critical temperature versus the reduced interlayer exchange interaction $J_3/|J_1|$ for $H/q|J_1| = 0.5$ and $J_2/|J_1| = 4.0$ for selected values of q. Results show that there are asymmetric second-order transition lines extending infinitely for $J_3/|J_1| \rightarrow \pm \infty$ which separate three distinct FM phases from the paramagnetic phase. Indeed, in this kind of phase diagrams, the critical temperatures present their high saturation values for large negative values of $J_3/|J_1|$, which are seen at higher $kT/|J_1|$ with higher q. As $J_3/|J_1|$ increases further, the critical temperatures then reach their maxima in the neighborhood of $J_3/|J_1| = 0$ and decrease to reach other saturation values for large positive values of $J_3/|J_1|$. Thus, left wings are seen at higher temperatures than the right ones, since $J_1 > 0$, $J_2 > 0$ favor the FM phase and $J_3 < 0$ favor the AFM phase while $J_1 > 0$, $J_2 > 0$ and $J_3 > 0$ favor FM phase (I). So phase (II) is more resistive to the temperature than phase (I). However, the maxima which follow up the occurence of phase (III) are due to a competition between positive and negative values of the bilinear exchange interaction parameters and the field. Consequently, the magnetizations persist for higher temperatures for phase (III). This type of phase diagram occurs for $J_2/|J_1| > 1 + 4H/q|J_1|$.

(*ii*)- Fig. 4b expresses phase diagrams for given $H/q|J_1| = 0.5$ and $J_2/J_1 = 2.0$ in ($J_3/|J_1|$, $kT/|J_1|$) plane. Numerical results clearly show that T_N's which appear constant for $J_3/|J_1| \rightarrow -\infty$, increase when we increase $J_3/|J_1|$ for negative values, pass through a maximum, and vanish at positive values of $J_3/|J_1|$. Thus, the right wings obtained in the previous figure now disappear and T_N-lines terminate in the phase region (IV) as we expected, since phase (IV) is AFM type and no second-order phase transitions are seen when the layers are linked with ESMF. It should be pointed out that, T_N increases with increasing coordination number q, meanwhile the crossing point moves towards right. The reentrant behavior is also seen for $q = 6$ only due to the existence of two T_N's. This type of phase diagram occurs for $2H/q|J_1|<J_2/|J_1| < 1 + 4H/q|J_1|$ while for $1 < J_2/|J_1| < 2H/q|J_1|$, T_N lines shift to negative direction with increasing values of the coordination number q. Thus, for $J_2/|J_1| = 2H/q|J_1|$, the T_N's go to zero temperature at zero $J_3/|J_1|$. These results are similar to those displayed on Fig. 3b of Ref. [23].

(*iii*)- Fig. 4c was obtained on the ($J_3/|J_1|$, $kT/|J_1|$) plane for $H/q|J_1| = 0.5$ and $J_2/J_1 = 0.5$. The phase diagrams are rather symmetric because their mirror images (not shown) about their center lines collapse into themselves. Indeed, two symmetrical second-order transition lines come out from $J_3/|J_1| = -q/2$ and $J_3/|J_1| = -3q/2$ at zero temperature and reach their maxima at $J_3/|J_1| = -q$. The wings obtained in the previous figures actually disappear with decreasing values of the exchange interaction parameter $J_2/|J_1|$ and

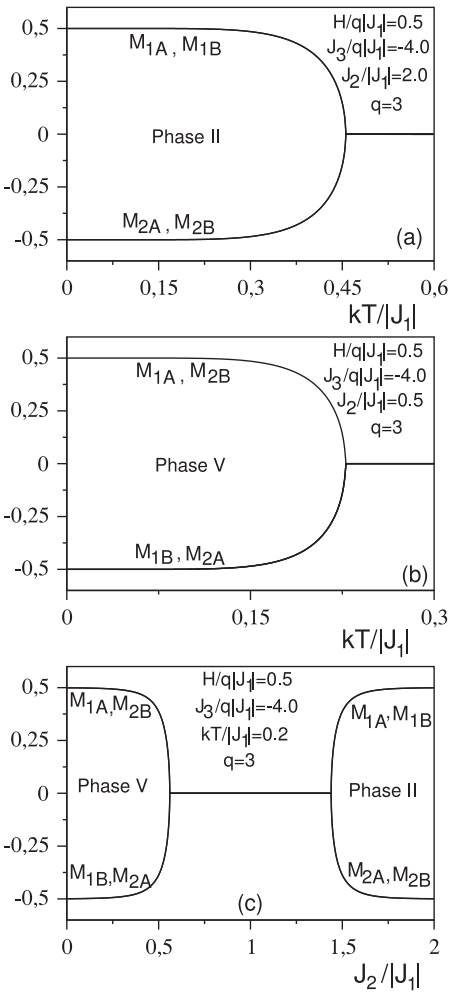

Fig. 3. Thermal and intralayer bilinear exchange interaction variations of the order-parameters for $q = 3$, $H/q|J_1| = 0.5$ and $J_3/q|J_1| = -4.0$ (a) $J_2/|J_1| = 2.0$; (b) $J_2/|J_1| = 0.5$ and (c) $kT/|J_1| = 0.2$.

the ordered phases which appear at low temperature shrink rapidly, while the (P) phase has an expansible tendency. This type of phase diagram occurs for $0 < J_2/J_1 < 1$.

We show in Fig. 4d, the phase diagrams in the $(J_2/|J_1|, kT/|J_1|)$ plane for $H/q|J_1| = 0.5$ and $J_3/q|J_1| = 4.0$. The T_N curves, which are seen at higher values for higher q, emerge from $J_2/J_1 = 3.0$ at $T = 0$ between phases (I) and (IV) with a little concavities. They also increase monotonically with the interaction parameter J_2/J_1 and separate phase (I) from the paramagnetic phase (P) at non-zero temperatures. The reentrant behavior is only obtained for $q = 6$. In the inset, one observes analogous phase diagrams as the one given in the main figure but phase (I) is replaced by phase (III). These phase diagrams are similar to those plotted in Fig. 3c of Ref. [23].

It can be clearly seen from Fig. 4e obtained in the $(J_2/|J_1|, kT/|J_1|)$ plane for $H/q|J_1| = 0.5$ and $J_3/q|J_1| = -4.0$ that the critical temperatures decrease linearly with decreasing $J_2/|J_1|$ until they reach the zero-temperature phase boundary between phases (II) and (V) at $J_2/J_1 = 1.0$. Afterwards, the new critical lines develop in the range $0 \leq J_2/|J_1| \leq 1$ and separate phase (V) from the paramagnetic phase (P). As far as we know, this behavior was not revealed in the case of uniform magnetic field acting on the layers [20]. It is important to note that these observations are consistent with the results shown in Fig. 3c. In the inset, our phase diagrams are similar to those of the main figure when phase (II) is replaced by phase (III) but, we actually do not observe any phase transition lines between phases (V) and (P). One of the most interesting feature shown in these phase diagrams, refers to the second-order phase transition lines between phases (V) and (P). Indeed, phase (V) is a AFM phase and the occurrence of second-order transition lines when the layers are under the influence of staggered magnetic field may be attributed to the competition between the bilinear exchange interaction parameters and the staggered field H.

In Fig. 4f, we present the dependence of kT/J_2 on J_1/J_2 for $H/qJ_2 = 0.125$ and $J_3/qJ_2 = -0.9$ (main figure) and $J_3/qJ_2 = 0.6$ (in the inset). At $J_2/J_1 = 0$, T_N's decrease with q, and also for fixed values of q, the behavior is not monotonic and T_N first decreases and eventually reaches a minimum and as J_2/J_1 increases, it becomes constant. However, T_N does not approach to 0 as $J_1/J_2 \to -\infty$ as it should. Similar results hold in ERR's method for Ising systems on a two-layer BL [23].

The phase diagrams of panels a-c of Fig. 5 are conctructed in the $(H/|J_1|, kT/|J_1|)$ plane for $J_2/|J_1| = 4.0$ and $J_3/q|J_1| = -4.0$

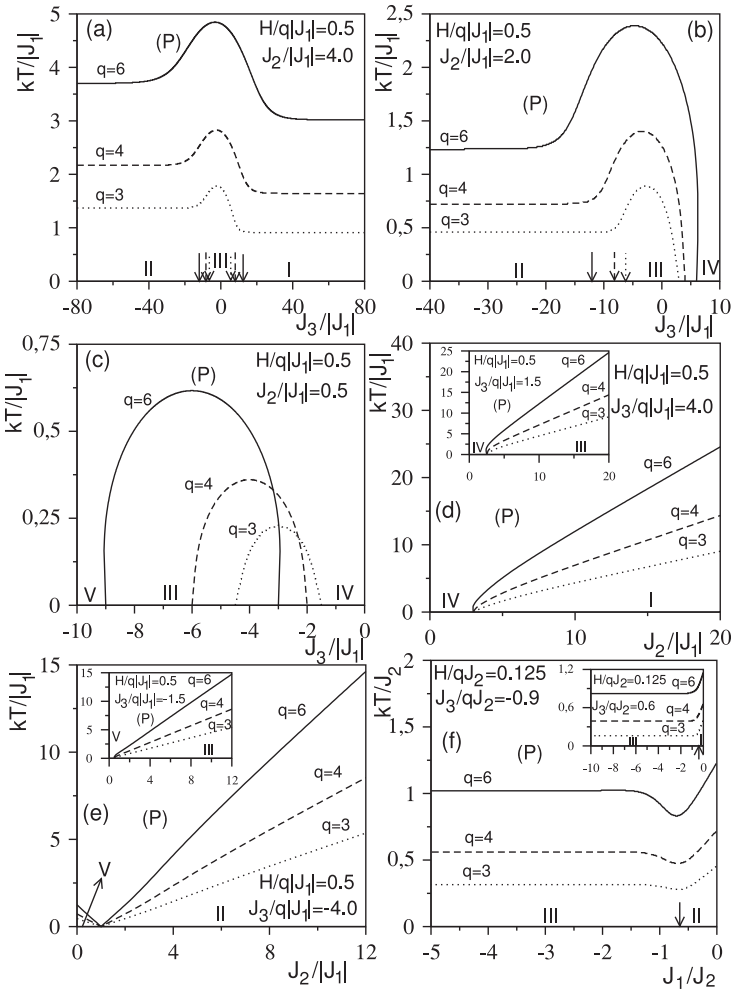

Fig. 4. The phase diagrams with $q = 3, 4$ and 6 (*i*) for $H/q|J_1| = 0.5$ on the $(J_3/|J_1|, kT/|J_1|)$ plane (a) $J_2/|J_1| = 4.0$, (b) $J_2/|J_1| = 2.0$ and (c) $J_2/|J_1| = 0.5$; (*ii*) for $H/q|J_1| = 0.5$ on the $(J_2/|J_1|, kT/|J_1|)$ plane (d) for $J_3/q|J_1| = 4.0$ and in the inset for $J_3/q|J_1| = 1.5$, (e) for $J_3/q|J_1| = -4.0$ and in the inset for $J_3/q|J_1| = -1.5$; (*iii*) for $H/qJ_2 = 0.125$ on the $(J_1/J_2, kT/J_2)$ plane (f) for $J_3/qJ_2 = -0.9$ and in the inset for $J_3/qJ_2 = 0.6$.

(Fig. 5a), $J_3/q|J_1| = 0.5$ (Fig. 5b), and $J_3/q|J_1| = 1.5$ (Fig. 5c). For these phase diagrams, the T_N-lines start from higher temperatures for higher q. In Fig. 5a, T_N's firstly increase with increasing $H/|J_1|$, pass through a maximum, and vanish at higher $H/q|J_1|$ for higher q's. The reentrant behavior is also obtained for $q = 6$.

In Fig. 5b,c the T_N's decrease as $H/|J_1|$ increases and then reach the zero-temperature axis at lower values of $H/|J_1|$ for lower q's.

According to Fig. 5a–c, one can see that, critical lines approach to the zero-temperature phase boundary between phases (III) and (IV) with a negative slope for $q = 3$ and 4, and with a positive slope for the coordination number $q = 6$. One may conclude that the reentrant behavior can be observed in the close vicinity of the ground-state boundary between phases (III) and (IV) for sufficiently high q's.

It can be seen from Fig. 5d that when H/J_2 increases, T_N's increase from $T_N = 0$ at $H/J_2 = 3q/4$, pass through a maximum at $H/J_2 = 5q/4$, and disappear again at $H/J_2 = 7q/4$. Corresponding phase diagrams are symmetric for $q = 3$, 4 but, not for $q = 6$ where the reentrant behavior is exhibited.

Fig. 5e,f are constructed on the $(J_3/J_2, kT/J_2)$ plane for fixed values of $J_1/J_2 = -0.5$ and varying $H/qJ_2 = 0.5$ and 1.0 respectively. Fig. 5e is similar to Fig. 4b, but actually the T_N's go to zero at zero J_3/J_2. Thus, phases (II) and (III) represent the ground state for $J_3/J_2 < 0$, while phase (IV) becomes the ground state for $J_3/J_2 > 0$. In Fig. 5f, phase diagrams are similar to those in Fig. 5e but as q increases, phase transition lines shift to the negative J_3/J_2 direction without changing their shapes.

5. Conclusion

In this work, we have studied the AFM/FM spin-1/2 Ising model in an external staggered magnetic field on a bilayer BL. The pairwise approach is used to derive the ERR's which is needed on the BL to obtain the solution of this model. By comparing energies of spin configurations at $T = 0$, the ground state phase diagrams are calculated and show very rich features. For any value of $H/q|J_1|$,

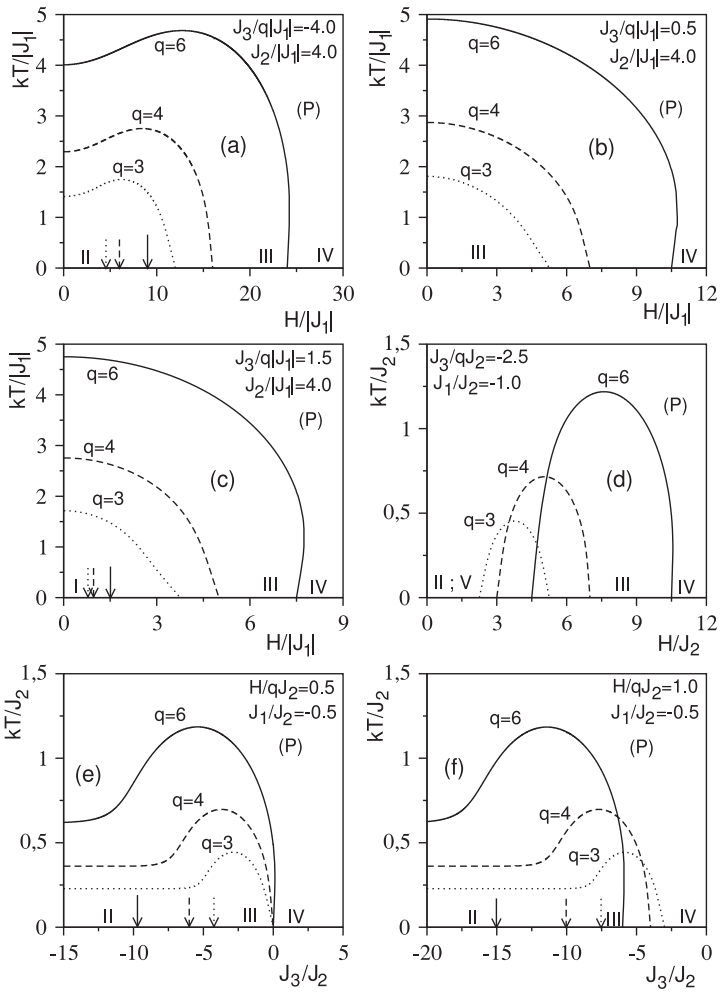

Fig. 5. The phase diagrams on the ($H/|J_1|$, $kT/|J_1|$) plane for $J_2/|J_1| = 4.0$ with $q = 3$, 4 and 6, (a) $J_3/q|J_1| = -4.0$, (b) $J_3/q|J_1| = 0.5$ and (c) $J_3/q|J_1| = 1.5$; (d) on the (H/J_2, kT/J_2) plane for $J_1/J_2 = -1.0$ and $J_3/qJ_2 = -2.5$ with $q = 3$, 4 and 6, and on the (J_3/J_2, kT/J_2) plane for $J_1/J_2 = -0.5$ with $q = 3$, 4 and 6 (e) $H/qJ_2 = 0.5$ and (f) $H/qJ_2 = 1.0$.

all thermodynamic phases are obtained in the ground state phase diagrams. This finding does not hold for values of $H/q|J_2|$. Thermal variations of the sublattice magnetizations also present interesting features. All the phase transitions lines are found in the form of the second-order phase transition type since the order parameters continuously vanish at the Néel temperature. This enables us to generate the temperature-dependent phase diagrams in different planes of the model parameters. The competition of the bilinear interaction parameters and the external staggered magnetic field has also been discussed in an induced magnetic ordering point of view. Some of our results have shown good resemblances with those reported in Refs. [20,23].

References

[1] H.J. Elmers, Int. J. Mod. Phys. B 9 (1995) 3115.
[2] Y. Benhouria, I. Essaoudi, A. Ainane, R. Ahuja, F. Dujardin, Chin. J. Phys. 54 (2016) 533.
[3] E. Albayrak, M. Karimou, Chin. J. Phys. 55 (2017) 1361.
[4] M. Karimou, E. Albayrak, A. Tessilimy, F. Hontinfinde, R. Yessoufou, Chin. J. Phys. 55 (2017) 2371.
[5] M.N. Baibich, J.M. Broto, A. Fert, F.N.V. Dau, F. Petroff, P. Eitenne, G. Creuzet, A. Friederich, J. Chazelas, Phys. Rev. Lett. 61 (1988) 2472. G. Binasch, P. Grunberg, F. Saurenbach, W. Zinn, Phys. Rev. B 39 (1989) 4828.
[6] J. Sayama, T. Asahi, K. Mizutani, T. Osaka, J. Phys. D 37 (2004) L1–L4.
[7] R.C. O'Handley, S.W. Sun, Phys. Rev. Lett. 66 (1991) 2798. G. Bochi, O. Song, R. C. O'Handley, Phys. Rev. B 50 (1994) 2043.
[8] J. Nogues, D. Lederman, T.J. Moran, I.K. Schuller, Phys. Rev. Lett. 76 (1996) 4624.
[9] L. Malkinski, T. O'Keevan, R.E. Camley, Z. Celinski, J. He, W.L. Zhou, M. Hecker, C.M. Schneider, J. Szade, D. Skrzypek, J. Vac. Sci. Technol. A 21 (4) (2003) 1162.
[10] K.W. Chou, A. Puzic, H. Stoll, G. Schütz, B.V. Waeyenberge, T. Tyliszczak, K. Rott, G. Reiss, H. Brückl, I. Neudecker, D. Weiss, C.H. Back, J. Appl. Phys. 99 (2006) 08F305.
[11] T.K. Yamada, E. Martinez, A. Vega, R. Robles, D. Stoeffler, A.L.V. de Parga, T. Mizoguchi, H. van Kempen, Nanotechnology 18 (2007) 235702.
[12] L.S. Huang, J.F. Hu, J.S. Chen, J. Magn. Magn. Mater. 324 (2012) 1242.

[13] J. Oitmaa, I.G. Enting, J. Phys. A, Math. Gen. 8 (1975) 1097.
[14] T. Bouziane, A. Belaaraj, Phys. Stat. Sol. (b) 214 (1999) 387.
[15] M. Jascur, A. Bobak, Phys. Rev. B 45 (1992) 9722.
[16] A.M. Ferrenberg, D.P. Landau, J. Appl. Phys. 70 (1991) 6215.
[17] K.H. Benneman, Magnetic Properties of Low-Dimensional Systems, Springer-Verlag, New York, 1986.
[18] W. Burkhardt, E. Eisenriegler, Phys. Rev. B 16 (1977) 3213. K. Ohno, Y. Okabe, Phys. Rev. B 39 (1989) 9764; Q. Jiang, Z. Y. Li, J. Magn. Magn. Mater. 80 (1989) 178 M. Wortis, N. M. Svrakic, Phys. Rev. B 15 (1977) 396.
[19] C.K. Hu, N.S. Izmailian, K.B. Oganesyan, Phys. Rev. E 59 (1999) 6489.
[20] E. Albayrak, A. Yigit, S. Akkaya, J. Magn. Magn. Mater. 320 (2008) 2241. E. Albayrak and A. Yigit, Acta Physica Polonica A 116 (2009) 128; E. Albayrak, Phys. Status Solidi B 246 (2009) 226.
[21] E. Albayrak, S. Yilmaz, Physica A 387 (2008) 1173. E. Albayrak, A. Yigit, Chin. Phys. B. 18 (2009) 4193.
[22] E. Albayrak, O. Canko, Physica A 373 (2007) 363. O. Canko, E. Albayrak, Phys. Rev. E 75 (2007) 011116.
[23] E. Albayrak, A. Yigit, Condens. Matter Phys. 12 (2009) 167.
[24] J. Kple, G.Y.H. Avossevou, F. Hontinfinde, Cent. Eur. J. Phys. 11 (2013) 1567.
[25] J.L. Monroe, Physica A 335 (2004) 563.
[26] E. Albayrak, S. Yilmaz, S. Akkaya, Physica A 381 (2007) 189.
[27] E. Albayrak, A. Yigit, Phys. Stat. Sol. (b) 242 (2005) 1510. E. Albayrak, A. Yigit, Physica A 349 (2005) 471. J. Kple, R. A. Yessoufou, F. Hontinfinde, Afr. Rev. Phys. 7 (2012) 319.
[28] A.Z. Akheyan, N.S. Ananikian, J. Phys. A 29 (1996) 721. N. S. Ananikian, A. R. Avakian, N. Sh. Izmailian, Physica A 172 (1991) 391; A. Z. Akheyan, N. S. Ananikian, Phys. Lett. A 186 (1994) 171 A. Z. Akheyan, N. S. Ananikian, JETP 107 (1995) 196.